IL NUOVO CIMENTO **41 C** (2018) 170
DOI 10.1393/ncc/i2018-18170-0

COLLOQUIA: IWM-EC 2018

Isospin effects in nuclear reactions

S. YENNELLO

Cyclotron Institute & Department of Chemistry, Texas A&M University - College Station, TX 77845, USA

received 3 December 2018

Summary. — The neutron-to-proton ratio of colliding nuclear systems can affect both the dynamics and thermodynamics that govern the reaction. These effects are a manifestation of the underlying nuclear interaction. Heavy-ion collisions can be used to probe nuclear material at finite temperatures and at densities away from saturation density. Comparison of experimental observables, from a diversity of reactions measured with various experimental apparatuses, with theoretical predictions, using different interactions, can help to constrain the nature of nuclear matter and enhance the accuracy of predictions of astrophysical phenomenon.

1. – Introduction

The origin of the elements is one of the fundamental questions in science today. All of the elements are made in nuclear reactions, starting from the p-p process to make the lightest elements, through fusion of progressively heavier elements to make medium-mass nuclei to neutron capture (and subsequent β decay) to make the heaviest elements. To fully understand the chemical composition of the universe detailed information about the myriad of the underlying nuclear reactions is required. Since the processes to produce the heavier elements are believed to take place in a very neutron-rich environment it becomes incumbent on us to understand how nuclear reaction processes are affected by the relative neutron richness of the environment in which they are taking place.

GW170817 produced light curves that are consistent with r-process nucleosynthesis [1] providing a link between merging neutron stars and element formation and much excitement about studying the origin of the elements in a multimessenger era. The calculations that link the light curves to the production of r-process nuclei are based on the current understanding of the extensive underlying nuclear reactions. Although there have been studies of heavy-ion reactions for many years, the focus on reactions with various neutron compositions now has an increased importance and appreciation. The particular questions I would like to address are how is the heat capacity of nuclear material affected by the neutron content; when nuclei collide what is the partitioning of the nuclear material, and on what time scale and to what degree is equilibrium achieved in these nuclear collisions. Additionally I will touch on how this informs the asymmetry energy of

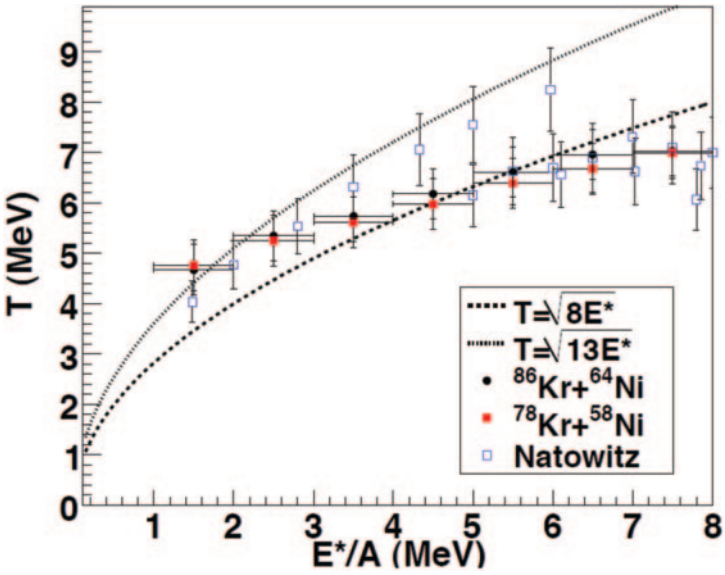

Fig. 1. – Temperature, extracted with the quadrapole fluctuation method, as a function of excitation energy from the reactions of ^{86}Kr + ^{64}Ni and ^{78}Kr + ^{58}Ni as a function of excitation energy.

the nuclear equation of state. When nuclei collide there is an exchange of neutrons and protons between the reacting partners and heating of the nuclear material as collisional energy gets transformed into excitation energy. The nuclear material, at normal nuclear density and liquid-like in its initial state, may expand to lower density and then re-cluster into fragments. Thus the dynamics of the collision, the heating of the nuclear material, the transport of nucleons between reaction partners, the clusterization and the eventual return to order from chaos are each subjects of intense study.

2. – Heating of nuclear material

A nuclear caloric curve was constructed by Pochodzalla [2] as a way to understand the heating of nuclear material by looking at the temperature, as measured through isotope ratios, *vs.* the excitation energy. This led to many experiments with an apparent diversity in results. A collection of these measurements was pulled together by Natowitz [3] and sorted on the mass of the system to reveal the dependence of the heating curve on the system size. Later work was done to investigate the dependence of the heating curve on the neutron composition of the system [4-6]. This work was limited by the looking only as a function of the neutron-proton content of the reacting system and not that of the systems from which the fragments are formed. Figure 1 shows the temperature extracted from the reactions of ^{86}Kr + ^{64}Ni and ^{78}Kr + ^{58}Ni as a function of excitation energy. The excitation energy was reconstructed from the energy balance of all detected fragments and neutrons in the quasiprojectile. The temperature was extracted from the quadrapole fluctuation method [5]. These data compare well with the Natowitz compilation (also shown in the figure). One can notice a slight offset of the two systems, but the data are certainly within error bars of each other. In a later study of ^{70}Zn+^{70}Zn, ^{64}Zn + ^{64}Zn and ^{64}Ni + ^{64}Ni, McIntosh was able to tease out the impact of the neutron

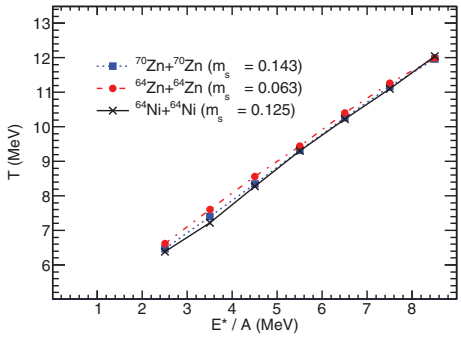

Fig. 2. – Temperature extracted with the quadrapole fluctuation method as a function of excitation energy using protons from the reactions of ^{70}Zn + ^{70}Zn, ^{64}Zn + ^{64}Zn and ^{64}Ni + ^{64}Ni, ($m_s = \frac{(N-Z)}{A}$).

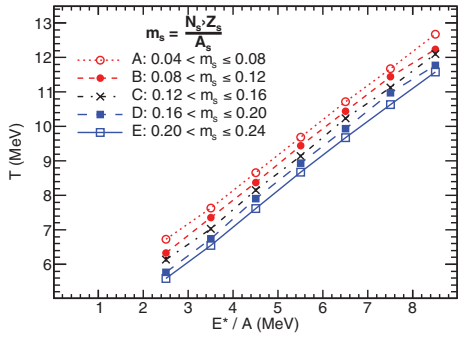

Fig. 3. – Temperature extracted with the quadrapole fluctuation method as a function of excitation energy using protons for bins in m_s, ($m_s = \frac{(N-Z)}{A}$).

content on the nuclear caloric curve by utilizing the complete reconstruction of the quasi-projectile in mass as well as charge [7-9]. Figure 2 shows the small dependence of the measured temperature on the N/Z of the reacting system. However when the fragmenting system is reconstructed from isotopically identified particles including measured neutrons the temperature dependence is much more apparent as shown in fig. 3. The striking new feature we observe is that increasing the neutron content lowers the temperature significantly for a given amount of internal energy. To date, theoretical models disagree on whether the temperature should rise, fall, or remain the same. This measurement of the composition dependence of the nuclear caloric curve can help constrain theoretical models and lead to an improved understanding of the nuclear equation of state. In order to probe the nuclear caloric curve at lower excitation energies, and eliminate any uncertainty from the neutron measurements the reactions of ^{78,86}Kr + C at 15, 25, 35 MeV/nucleon were measured with the FAUST array and the Quadrupole Triplet Spectrometer. The analysis of these data is underway [10].

3. – Partitioning of nuclear material

To first order the isotope abundance of fragments produced in a reaction will be reflective of the neutron-proton content of the reacting system. This is shown in fig. 4 for carbon fragments emitted from the reactions of ^{58}Fe and ^{58}Ni on targets of ^{58}Fe and

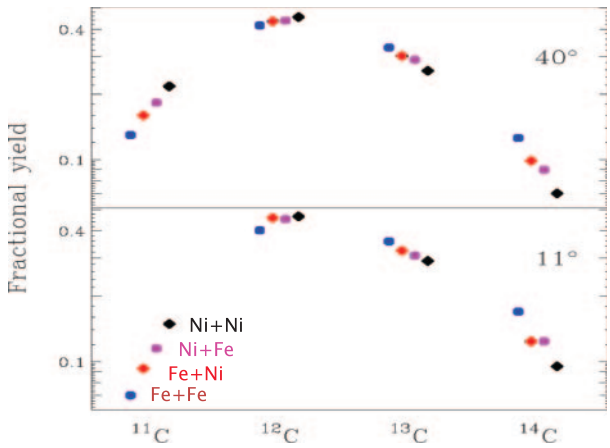

Fig. 4. – Isotopic abundance of carbon fragments emitted from the reactions of ^{40}Ca, ^{40}Ar and ^{40}Cl were reacted on target of ^{58}Fe and ^{58}Ni at 30 MeV/nucleon. Data taken from [11].

^{58}Ni at 30 MeV/nucleon [11]. The more neutron-rich systems produce higher fractions of neutron-rich isotopes relative to the less neutron-rich systems. The effect is most noticeable in the isotopes further from $N = Z$.

Since the asymmetry energy of nuclear material is a function of density, systems with excess numbers of neutrons experience an additional driving force that preferentially moves neutrons, relative to protons, into the low-density phase. This has been observed in measurements of neutrons in the neck of heavy-ion collisions [12,13]. $A = 3$ fragments are particularly sensitive to the asymmetry energy as they are more likely formed from low-density nuclear material rather than from nuclear material at saturation density. In

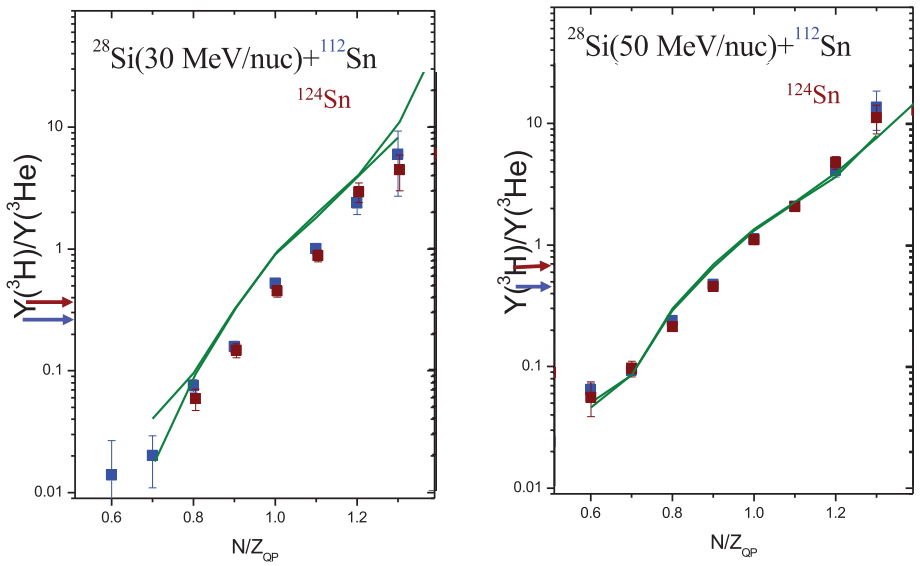

Fig. 5. – Ratio of ^{3}H to ^{3}He as a function of N/Z_{QP} for fragmentation of ^{28}Si + ^{112,124}Sn at 30 MeV/nucleon and 50 MeV/nucleon. Lines represent a hybrid DIT/SMM calculation.

the work of Veselsky [14, 15], the ^{3}H/^{3}He ratio of fragments from reconstructed QPs has a much larger dependence on the N/Z of the composite system then would be predicted solely from the numerics of the numbers of available neutron and protons as shown in fig. 5. The blue points represent the reactions with the ^{112}Sn target while the red points are the reactions on the ^{124}Sn target. The ratio of ^{3}H to ^{3}He is a function of the N/Z of the reconstructed quasiprojectile and is independent of the target. However if one had observed the ratio of ^{3}H to ^{3}He as a function of the reacting system one would note a difference between the ratios from the reaction on the two different targets as indicated by the arrows on the axis of the respective colors of the points. This again points out the ability of the reconstructed quasiprojectiles to discern effects of the neutron content of the system more sensitively than the reacting system. The relationship of the ratio of ^{3}H to ^{3}He to the N/Z of the reconstructed quasiprojectile is stronger at lower energy and independent of the colliding system as long as the data is sorted as a function of the fragmenting system.

In addition to the N/Z effect, the formation of clusters is energetically favored at low density [16, 17]. The impact of this on asymmetry energy will be shown later. Very large nuclear systems exhibit clustering in various forms as a function of density that can be compared to different shapes of nuclear pasta [18].

4. – Equilibration chronometry

In studying nuclear reactions it becomes important to understand what degrees of freedom come to equilibrium, or to what extend the system has evolved toward equilibrium and the timescale on which equilibrium is achieved. While there are various degrees of freedom in which one could consider the equilibrium, it was shown that at Fermi energies the isospin degree of freedom relaxes faster than the momentum degree of freedom [19]. At energies of 100 MeV/nucleon and above the momentum timescale is faster.

Isospin equilibration can be studied in multiple ways, by measuring translucency in central collisions; diffusion between target and projectile in peripheral collisions; or transport in deformed nuclear systems, as shown in fig. 6. The first experiments to show that there was incomplete mixing is shown in fig. 7 [20]. In this experiment, beams of ^{40}Ca, ^{40}Ar and ^{40}Cl were reacted on targets of ^{58}Fe and ^{58}Ni at 53 MeV/nucleon. The reactions of Ar + Ni and Ca + Fe both yield composite systems of 46 protons and 52 neutrons. However the isobaric ratios observed for fragments are not the same, indicating that there is incomplete equilibration in the reaction. Figure 7 shows the ratios of ^{10}Be/^{10}B fragments detected at 40° in the laboratory. The lines connect the data from a common target. In a follow-up experiment probing lower energies we see the onset of equilibrium at 33 MeV/nucleon as measured by the isobaric ratios of intermediate-mass fragments as shown in fig. 8 [21]. At 33 MeV/nucleon the ratios of ^{7}Li/^{7}Be, ^{10}Be/^{10}B and ^{11}B/^{11}C are the same for the ^{40}Ar + ^{58}Ni and ^{40}Ca + ^{58}Fe reactions, which is consistent with equilibrium. While at 45 MeV/nucleon the ratios from the ^{40}Ar + ^{58}Ni reaction are different than those from the ^{40}Ca + ^{58}Fe reaction, which is an indication of fragmentation before complete equilibration. Again the lines connect data from a common target.

Most recently the study of NZ equilibration has been advanced by investigating the deformed projectiles that are formed in the reaction of ^{70}Zn + ^{70}Zn, ^{64}Zn + ^{64}Zn, ^{64}Ni + ^{64}Zn and ^{64}Ni + ^{64}Ni [22, 23]. This work extends the work of [24] and [25] In these reactions, a projectile collides with a target nucleus to form a di-nuclear complex. The projectile rotates around the target forming a low-density neck region in between.

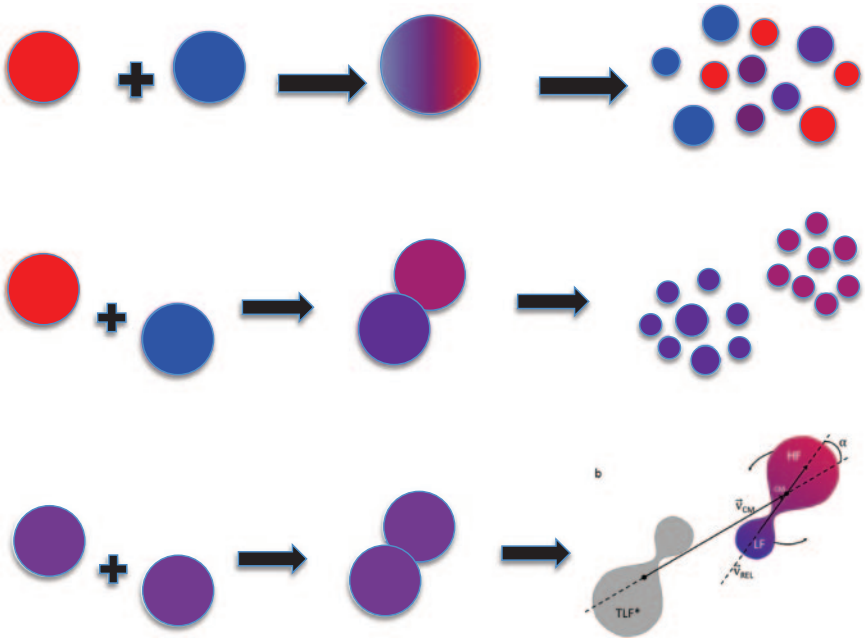

Fig. 6. – Mechanisms for equilibration as measured by translucency in central collisions; diffusion between target and projectile in peripheral collisions; or transport in deformed nuclear systems.

Because it is low density, neutrons preferentially flow to the neck making it more neutron-rich matter. (The extent to which this happens is related to the density dependence of the asymmetry energy.) As the excited projectile-like fragment (PLF*) continues to move away from the excited target-like fragment (TLF*) the di-nuclear complex stretches with the largest fragments going most forward or backward and smaller fragments being formed out of the neck region. At some point the nuclear system will break into two pieces with the PLF* separating from the TLF*. Both of these will be highly deformed. It is possible that the deformed PLF* will be pulled back together or it could fragment in to two pieces here called the Heavy Fragment (HF) and Light Fragment(LF). The relative

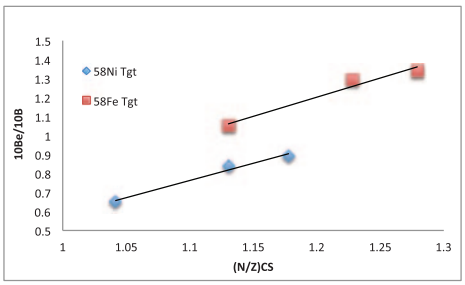

Fig. 7. – Ratio of ^{10}Be/^{10}B measured at 40° as a function of the N/Z of the combined target and projectile system from the reactions of ^{40}Ca, ^{40}Ar, ^{40}Cl + ^{58}Fe, ^{58}Ni at 53 MeV/nucleon. Lines are linear fits to the data points for a given target. Statistical error bars are smaller than the size of the points. Data taken from [20].

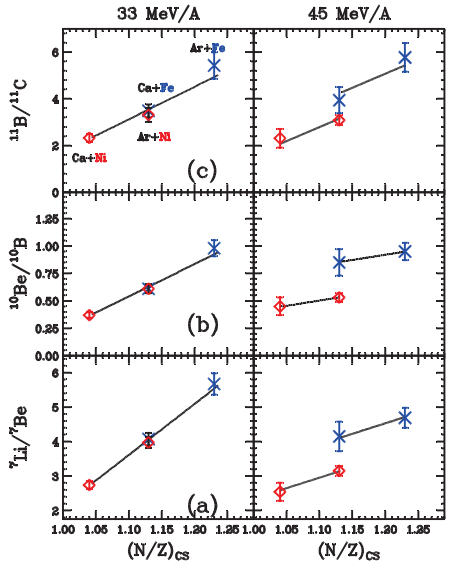

Fig. 8. – Isobar ratios plotted as a function of the N/Z of the combined target and projectile system. (a) $A = 7$, (b) $A = 9$, (c) $A = 11$. Lines are linear fits to the data points for a given target. Data taken from [21].

probability of these two outcomes is related to the strength of the mean field. Since there is angular momentum the PLF* will rotate away from the axis of separation. In fig. 6 we show the heavy fragment separating from the light fragment. The extent of the rotation is a measure of the time that the heavy fragment stayed in contact with the light

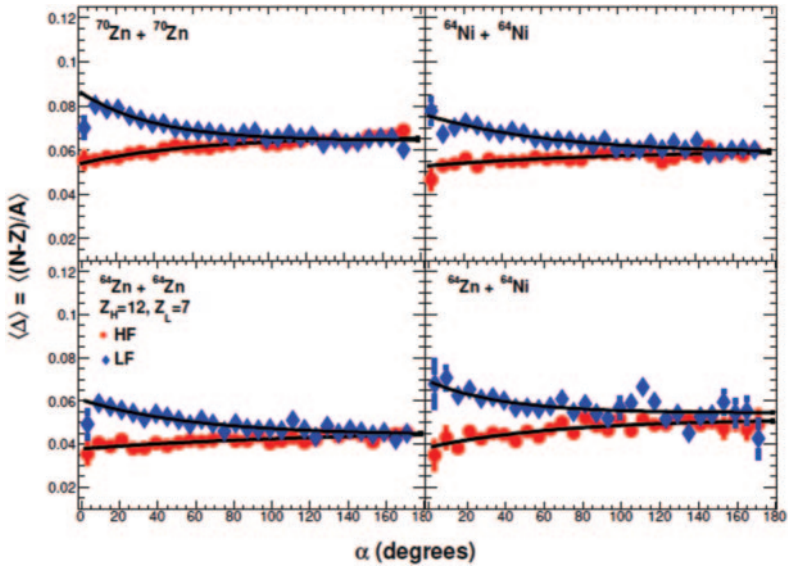

Fig. 9. – Neutron richness *vs.* decay alignment for different systems. The heavy fragment is shown in blue and the light fragment is shown in red. The lines are exponential fits to the data. Data has been taken from [22].

fragment before separation, and hence can be used as a clock for the NZ equilibration. Since the light fragment came from the neutron-rich neck region and the heavy fragment came from the more neutron/proton balanced part of the PLF* there is flow of neutrons from the light fragment to the heavy fragment in an attempt to reach NZ equilibrium as the chemical potentials of neutrons and protons are not equal. When the heavy fragment separates from the light fragment the exchange of neutrons (equilibration) stops as does the rotation (clock). Since we measure both the neutron and proton content of both the heavy fragment and the light fragment, as well as the angle of rotation, we can watch the NZ equilibration taking place in real time, which is on the order of zeptoseconds. We find that the change in neutron richness as a function of time follows an exponential behavior which is indicative of a first-order rate law. Figure 9 shows this behavior for four different systems varying in N/Z and mass [22]. A detailed discussion of this work can be found elsewhere in these proceedings [26]. An extension of this study of neutron-proton equilibration in dynamically deformed nuclear systems to investigate the correlations between the three largest fragments coming from the excited projectile-like fragment is underway [27].

5. – Effect on the asymmetry energy of EOS

Comparing experimental observables to calculations using different underlying potentials (that exhibit different density dependences of the asymmetry energy) can help to constrain the symmetry energy [28]. While much success has been achieved by this mechanism it is particularly useful if comparisons are made to multiple models to reduce the model sensitivity of the results. One example of this is the work by Kohley looking at fragment flow [29] as shown in fig. 10. The ratio of the transverse collective flow of intermediate mass fragments measured in the reactions of ^{70}Zn + ^{70}Zn, ^{64}Zn + ^{64}Zn,

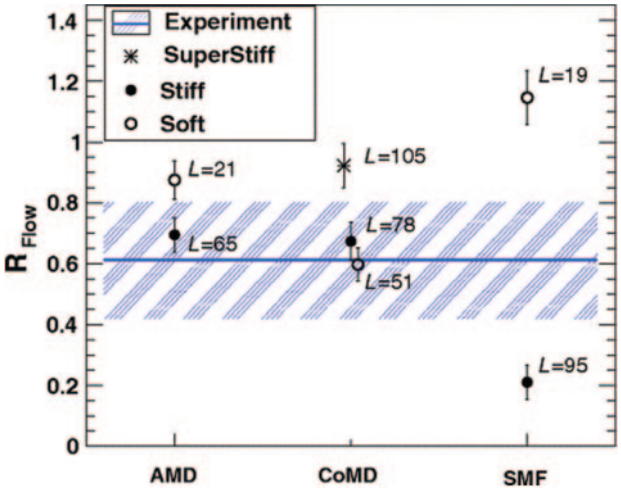

Fig. 10. – R_{flow} value from the nucleon-averaged flow of the midperipheral reactions is shown for the different symmetry energy parametrizations of the AMD, CoMD, and SMF models. The corresponding symmetry energy slope (L) is shown next to each calculation. The experimental value is represented by the solid blue line with the statistical uncertainty shown as the hatched blue area. Data has been taken from [29].

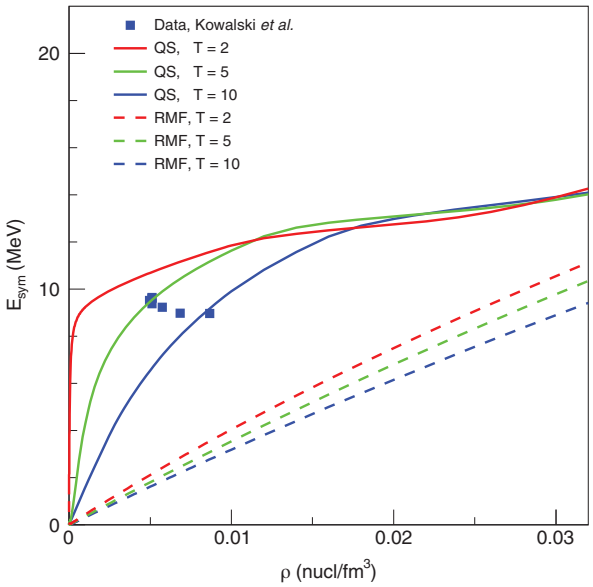

Fig. 11. – Symmetry energy as a function of density. Experiment [17] compared with predictions from QS model [30].

^{64}Ni + ^{64}Zn and ^{64}Ni + ^{64}Ni are compared with predictions from three different theoretical models with underlying potentials that exhibit a range of asymmetry energies. Note that for all three models the experimental data suggests an L value of 0.6 ± 0.2. Rather than comparing experimental results to theoretical calculations to evaluate the asymmetry energy, a more direct method would be for the density to be measured in the same experiment as the asymmetry energy. This has been done by Natowitz as shown in fig. 11. The figure clearly shows that the quasiparticle mean-field approach (RMF without clusters) disagrees strongly with the symmetry energy extracted from the experimental data while the QS approach shows much better agreement. It is imperative that theoretical models consider medium-dependent cluster formation in order to accurately describe the low-density dependence of the symmetry energy observed experimentally. A density dependence of the symmetry energy that shows vanishing symmetry energy at zero density and a linear increase with density cannot be correct because correlations and cluster formation are necessary ingredients in any calculation of the low-density region [30].

6. – Summary

There are various effects of the relative neutron content on nuclear reactions whether they be heavy-ion reactions measured in the laboratory or stellar events. It is important to continue to pursue the knowledge of the dynamic and thermodynamics of heavy-ion collisions, particularly with respect to the NZ degree of freedom and to compare the constraints set on the asymmetry energy from heavy-ion collisions with those extracted from the multimessanger data as discussed elsewhere in these proceedings [31].

* * *

This material is based upon work supported by the U.S. Department of Energy, Office of Science, Office of Nuclear Physics under Award Number DE-FG02-93ER40773 and the Welch Foundation under grant A-1266. We are indebted to the staff at the Texas A&M Cyclotron Institute for providing the high quality beams that made this work possible and the many fruitful conversations with numerous colleagues throughout the field.

REFERENCES

[1] Drout M. R. *et al.*, *Science*, **358** (2017) 1570.
[2] Pochodzalla J. *et al.*, *Phys. Rev. Lett.*, **75** (1995) 1040.
[3] Natowitz *et al.*, *Phys. Rev. C*, **65** (2002) 034618.
[4] Sfienti C. *et al.*, *Phys. Rev. Lett.*, **102** (2009) 152701.
[5] Wuenschel S. *et al.*, *Nucl. Phys. A*, **843** (2010) 1.
[6] Wuenschel S., *Temperature and scaling studies from projectile fragmentation of* $^{86,78}Kr+^{64,58}Ni$ *at 35 MeV/nuc*, PhD Thesis, Texas A & M University (2009).
[7] McIntosh A. B. *et al.*, *Phys. Lett. B*, **719** (2013) 337.
[8] McIntosh A. B. *et al.*, *Eur. Phys. J. A*, **50** (2014) 35.
[9] McIntosh A. B. *et al.*, *Phys. Rev. C*, **87** (2013) 034617.
[10] McIntosh A. *et al.*, *Measurement of Kr+C @ 15, 25, 35 MeV/nuc*, Texas A&M Cyclotron Institute Progress in Research (2016).
[11] Ramakrishnan E. *et al.*, *Phys. Rev. C*, **57** (1998) 1803.
[12] Thériault D. *et al.*, *Phys. Rev. C*, **71** (2005) 014610.
[13] Thériault D. *et al.*, *Phys. Rev. C*, **74** (2006) 051602.
[14] Veselsky M. *et al.*, *Phys. Rev. C*, **62** (2000) 064613.
[15] Yennello S. *et al.*, *Nucl. Phys. A*, **681** (2001) 317.
[16] Sumiyoshi K. and Röpke G., *Phys. Rev. C*, **77** (2008) 055804.
[17] Kowalski S. *et al.*, *Phys. Rev. C*, **75** (2007) 014601.
[18] Horowitz C. *et al.*, *Phys. Rev. Lett.*, **114** (2015) 031102.
[19] Li B.-A. and Ko C. M., *Phys. Rev. C*, **57** (1998) 2065.
[20] Yennello S. *et al.*, *Phys. Lett. B*, **15** (1994) 321.
[21] Johnston H. *et al.*, *Phys. Lett. B*, **371** (1996) 187.
[22] Rodriguez Manso A. *et al.*, *Phys. Rev. C*, **95** (2017) 044604.
[23] Jedele A. *et al.*, *Phys. Rev. Lett.*, **118** (2017) 062501.
[24] Brown K. *et al.*, *Phys. Rev. C*, **87** (2013) 061601.
[25] Stiefel K. *et al.*, *Phys. Rev. C*, **90** (2014) 061605.
[26] Manso A. R. *et al.*, these proceedings.
[27] Manso A. R. *et al.*, *Neutron-proton equilibration in dynamically deformed nuclear systems: multifragmentation*, Texas A&M Cyclotron Institute Progress in Research (2018).
[28] Tsang M. *et al.*, *Phys. Rev. C*, **86** (2012) 015803.
[29] Kohley Z. *et al.*, *Phys. Rev. C*, **85** (2012) 064605.
[30] Hagel K., Natowitz J. B. and Röpke G., *Eur. Phys. J. A*, **50** (2014) 39.
[31] Lukasik J., these proceedings.